

**Physical Model Investigation of Air Release
through Riser in Proposed District of
Columbia CSO Storage Tunnel**

**James W. Lewis, Steven J. Wright, and
Jose G. Vasconcelos**

**University of Michigan
Civil & Environmental Engineering
UMCEE 09-06
December 2009**

1 Background

1.1 Introduction and Summary

A physical model study investigated interactions between air and water within a proposed underground combined sewer overflow (CSO) tunnel. The specific issue is the release of pockets of trapped air from the tunnel through a riser that is in a surcharged state, such that the bubble must pass through water that stands in the riser shaft. Geyser events have occurred in existing systems through relatively large diameter risers (Wright et al. 2009, Guo and Song 1991). Previous work by the authors shows that the release of air pockets through vertical shafts can lead to geyser events. The current riser configuration involves a 23 foot diameter vertical riser expanding to a diameter of 45 foot at a distance of one tunnel diameter above the crown of the 23 foot diameter tunnel. The scale ratio based on the diameter of the model constructed at the University of Michigan Hydraulics Lab to the prototype tunnel is 1:73.6. The ability of the prototype tunnel and riser layout to prevent geyser events was investigated.

Summary of Findings:

- The diameter expansion within the riser reduced the geyser strengths an average of roughly 20% compared to the constant diameter case.
- Two methods of measuring the geyser strength are distinguished, namely the surface level of the water and the splash height.
- The geyser strength increased as the static water level in the vertical shaft increased.
- Splashing of water droplets rose significantly higher than the free surface level of the liquid.
- The phenomenon of flooding instability in the large prototype system would carry a mixture of air and water higher than the laboratory observations indicate.
- Following the release of a large air pocket, a low local pressure may develop that initiates a flow of water toward the riser. The inertia of this liquid causes an overshoot of the equilibrium pressure in the system, qualitatively explaining the behavior of the free surface level in the riser.
- Inertial surge generated by the release of air pockets is expected to be less of a concern than the splashing of the geyser event in the prototype system.

1.2 Air Entrapment

Air must be vented from a filling storage tunnel; when filled at low rates, the air is displaced gradually as the water level rises gradually in the tunnel. However, large storms may cause the conduit to be filled sufficiently rapidly resulting in pipe-filling or free surface bores that propagate through the

system. Vasconcelos and Wright (2006) discuss a number of ways in which this rapid filling process can result in the entrapment and pressurization of large air pockets and Wright, et al. (2008) discuss laboratory observations from experiments following up on preliminary numerical simulations of the proposed Washington DC storage tunnel system, showing that free surface bores reflecting off tunnel transitions may trap very large air volumes. For example, pressurization may occur at multiple points between riser shafts due to the collisions of free surface bores, creating trapped volumes of air. Furthermore, these large volumes of air may subdivide into multiple discrete pockets as they migrate within the tunnel.

1.3 Air Pocket Release

Trapped air pockets may migrate in either direction within near-horizontal conduits. The work of Benjamin (1968) shows that the required flow velocity to prevent the upstream migration of air pockets is equal to $0.54\sqrt{gD}$ where D is the diameter of the main tunnel. Therefore, the prototype 23 foot diameter tunnel would require a velocity of over 14.7 ft/sec, or a flow rate of over 6,000 cfs, to prevent the upstream migration of air pockets. This flow is unrealistic and therefore large trapped air pockets should be able to migrate up the main tunnel due to their buoyancy until they reach a vertical shaft.

If the vertical shaft is in a surcharged state, the momentum of a rising air pocket may be capable of lifting liquid above it. The rising air pocket tends to occupy the center of the vertical shaft while the liquid forms a thin film layer flow downward around the perimeter of rising air (Davies and Taylor 1950). The pressurized air pocket is capable of rising with significant velocities proportional to the square root of the diameter of the shaft and transferring some of this upward momentum to the “slug” of liquid above it. The slug flow regime occurs when the air rises in discrete pockets with liquid slugs between these pockets. This physical process of lifting the liquid significant distances during slug flow is also relevant to the subject of air-lift pumps (Nicklin 1963). An increase to the flow of air increases the counter-current shear between the upward moving air and the downward flowing water. Surface waves may develop at this interface (Hewitt and Wallis 1963) and become unstable due to the increased shear. Flooding instability occurs when the liquid from the wave crests experiences enough shear to be entrained in the upward air flow. This physical process is very difficult to study at the laboratory scale because a large diameter shaft would be required to produce air velocities high enough to cause flooding instability. The authors believe this phenomenon may be an important factor in large scale systems, however, resulting in the discharge of an air/water mixture from the top of a riser during a geyser event.

1.4 Surge Effects

The release of large air pockets causes a change to the local pressure which can result in surge effects within the riser shaft. Wright, et al. (2009) present pressure measurements made during geyser events in a prototype stormwater system that show sudden pressure drops as the geyser forms. It is presumed that after release of the air, water flows back into the riser with a resulting inertial surge. In general, these surges are less influential than the surge mechanisms associated with the rapid filling of the main tunnel. However, tunnel filling mechanisms were not studied in the current investigation. After a large air pocket is ventilated the water level in the vertical riser will drop below a level consistent with the equilibrium pressure of the system due to the change in volume associated with the size of the air pocket. This lower water level in the riser acts as a pressure gradient which causes a surge of water to flow toward the riser. The surge height can be found as a function of the inertia and momentum changes in the system. Equations 1 and 2 show the conservation of mass and momentum using a stationary control volume approach.

$$\text{Conservation of Mass:} \quad \frac{d}{dt} \int_{\mathcal{V}} \rho d\mathcal{V} + \int_S \rho(\bar{v} \cdot \hat{n}) dS = 0 \quad (\text{Eq. 1})$$

$$\text{Conservation of Momentum:} \quad \frac{d}{dt} \int_{\mathcal{V}} \rho \bar{v} d\mathcal{V} + \int_S \rho \bar{v}(\bar{v} \cdot \hat{n}) dS = \sum \bar{F} \quad (\text{Eq. 2})$$

where ρ is the density, \mathcal{V} is the control volume, S is the surface of the control volume, \bar{v} is the velocity of the fluid, \hat{n} is the unit vector which is normal to the surface, and \bar{F} represents all of the body and surface forces acting on the control volume. These conservation equations can be used to predict the oscillations within the riser caused by local sudden changes to the water level.

1.5 Previous Investigation

The authors conducted a similar investigation in the fall of 2008 that focused on studying some of the basic mechanisms of air / water interactions during air pocket release (Lewis, et al. 2009). The main tunnel was connected to a reservoir at the upstream boundary and completely closed at the downstream end. Air was continuously injected into the main tunnel near the upstream end of the tunnel. The air migrated to the vertical riser located near the downstream end of the tunnel and ventilated at that location. Objectives of the study were to investigate air migration behavior, determine which air release scenarios are most problematic, and compare the effectiveness of a proposed diameter expansion within the riser.

Some qualitative conclusions were made from the fall 2008 investigation. Large air pockets migrated faster than smaller ones and the propagation distance was large enough to cause many of the

small air bubbles to coalesce into larger bubbles. Large air pockets were more problematic than smaller ones in causing geyser events because they were able to swiftly accelerate a slug of liquid in front of them. The study also showed that the diameter expansion successfully reduced the strength of geyser events under certain conditions. The expansion strategy was most effective when it was located lower in the vertical shaft and with a greater expansion ratio between the expanded diameter and the original riser diameter. Some of the results of the previous study were influential in shaping the details of the current investigation.

2 Experimental Investigation

2.1 Experimental Setup

The experimental setup of the current investigation is shown in Figure 1 and is very similar to the setup used in the fall 2008 investigation. A large reservoir is connected to the upstream end of the tunnel where the water surface can be adjusted and maintained at a constant level. The main tunnel consists of 24 feet of 3.75 inch diameter (I.D.) clear acrylic pipe constructed on a horizontal slope and capped at the downstream end. An elbow joint pointing downward is located at the upstream end to prevent air from being released into the reservoir. A T-joint is located at the downstream end of the tunnel with a 3.75 inch diameter vertical riser attached. A diameter expansion occurs at a distance of 3.75 inches (one tunnel diameter, or $1D$) above the crown of the main tunnel, expanding the riser diameter to 7.5 inches. The vertical shaft in the 2008 investigation was much smaller, 1.75 in. diameter. The tested vertical locations of the expansion were 16 and 40 in. (model) above the invert of the main tunnel, which is much higher than the current investigation of 7.5 in (model). Note that the expanded diameter of the prototype layout is 45 feet and the expansion diameter in the lab model would be 46 feet at the prototype scale; this difference is due to the need to use available material sizes and is not considered to have any significant effects on the study conclusions. Air is injected at a location 9.5 feet from the reservoir, or 14.5 feet away from the riser. Measurements were taken using a digital video camera capable of 30 frames per second.

2.2 Procedure

A set of experiments was performed by adjusting two variables: the air injection rate and the initial water level within the system. Table 1 shows the combinations of four water levels and two air flow rates tested. The lowest water level corresponds to a slightly surcharged main tunnel. The second surcharge level is halfway between the main tunnel and the location of the riser expansion. The third level is just slightly above the expansion location and the fourth level is one tunnel diameter above the

expansion. Once the water level was established for each experiment, the air injection was initialized. Video recordings of 3 minutes in length were taken for each of the 8 trials. These video recordings were used to measure the geyser behavior within the vertical shaft.

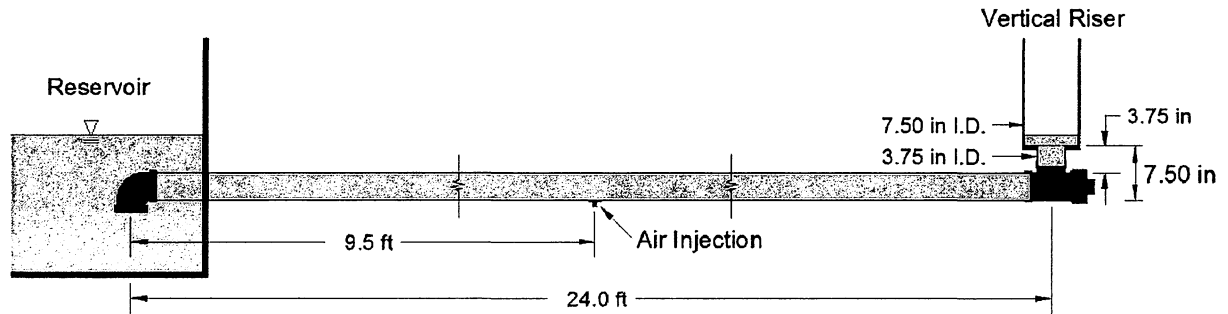


Figure 1. Sketch of Experimental Setup

Table 1. List of Experimental Conditions

Label	Air flow rate (L/min)	Initial Water Level (ft., model)	Initial Water Level (ft., prototype)
1A	8	0.34	25
1B	25	0.34	25
2A	8	0.47	34.5
2B	25	0.47	34.5
3A	8	0.65	48
3B	25	0.65	48
4A	8	0.94	69
4B	25	0.94	69

3 Results

3.1 Air Migration

Several observations were made regarding the interactions between air and water within the main tunnel of the system. The air formed a nearly continuous layer along the crown of the pipe because the tunnel was capped downstream preventing water flow. Assuming the air flow is directly scalable between the model and prototype based on the diameter of the main tunnel, the air flow rates of 8 and 25 L/min would be 219 and 685 ft³/s in the prototype, respectively. The low air flow rate approximately occupied the top 15% of the depth of flow or 9% of the cross sectional area, while the high air flow rate occupied

roughly 33% of the flow depth or 29% of the main tunnel area. These air flow rates represent a reasonable range of the expected air concentrations due to entrapment and are significantly larger than the expected concentrations due to air entrainment at a drop-shaft. Indeed, the draft document for the IIHR study (IIHR 2009) shows the largest rate of air entrainment of 450 ft³/min during 1100 MGD of water flow. This air concentration of 1.4% is roughly an order of magnitude below the 9% air concentration approximated from video observations in this study. A maximum threshold of air flow within a tunnel system can be found using the Benjamin (1968) findings for air intrusions. The air may occupy a maximum depth of one half of the tunnel diameter with an intrusion velocity of $0.54\sqrt{gD}$, corresponding to an air flow rate of 112 L/min in the physical model, or 3063 ft³/s prototype. Occasionally, the air would form into a large volume discrete pocket having a bore associated with the tail. The bore filled the entire main tunnel and was followed by a distinct head to the following air pocket, as seen in Figure 2. These air pockets were large as they reached the vertical riser. From previous investigations, these large air pockets are associated with the most problematic geyser events. It is difficult to approximate the quantity of air that would need to be trapped in discrete pockets in order to exhibit a comparable behavior of air release as observed in this investigation.

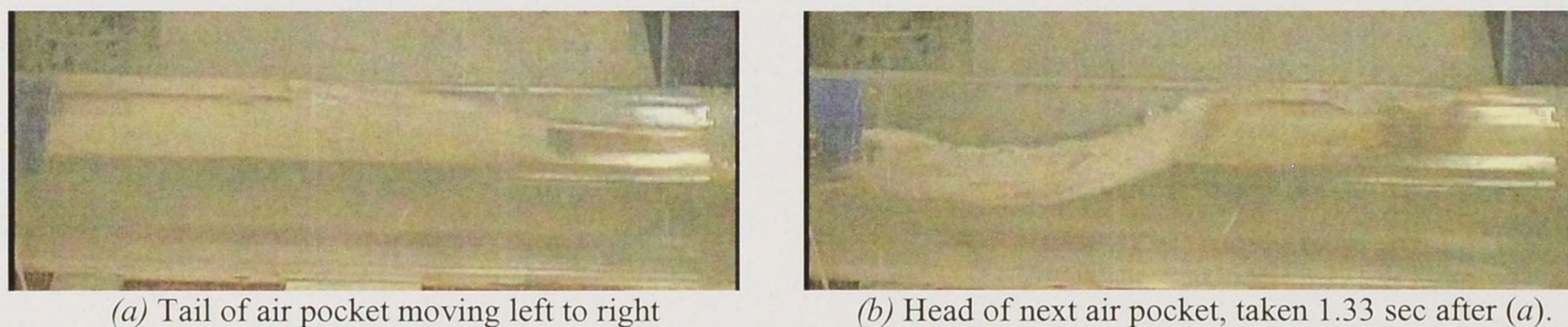


Figure 2. Images of Air Pockets in Main Tunnel, air flow rate of 25 L/min.

3.2 Air Release

The diameter expansion effectively influenced the vertical release of the air pockets within the riser. Figure 3 shows a large air pocket expanding in all directions as it enters the larger diameter of the riser expansion. This volumetric expansion in the radial direction limits the continued increase of upward momentum of the rising air, thus decreasing the strength of the geyser event. This transition also serves to allow water to flow around the rising air pocket more easily than for a constant diameter riser. Figure 3 shows what appears to be an expanding bubble but the system pressures are so low that compressibility effects are negligible and the air is simply being fed from the air remaining in the horizontal pipeline. Once the top of the air pocket breaks through the free surface of the water, the behavior becomes chaotic as subsequent air arrives and is ventilated quickly through the disrupted water in the riser. This chaotic

behavior prevents any slugs of liquid from being lifted within the riser but may increase the amount of water droplets that are entrained in the upward flowing air.

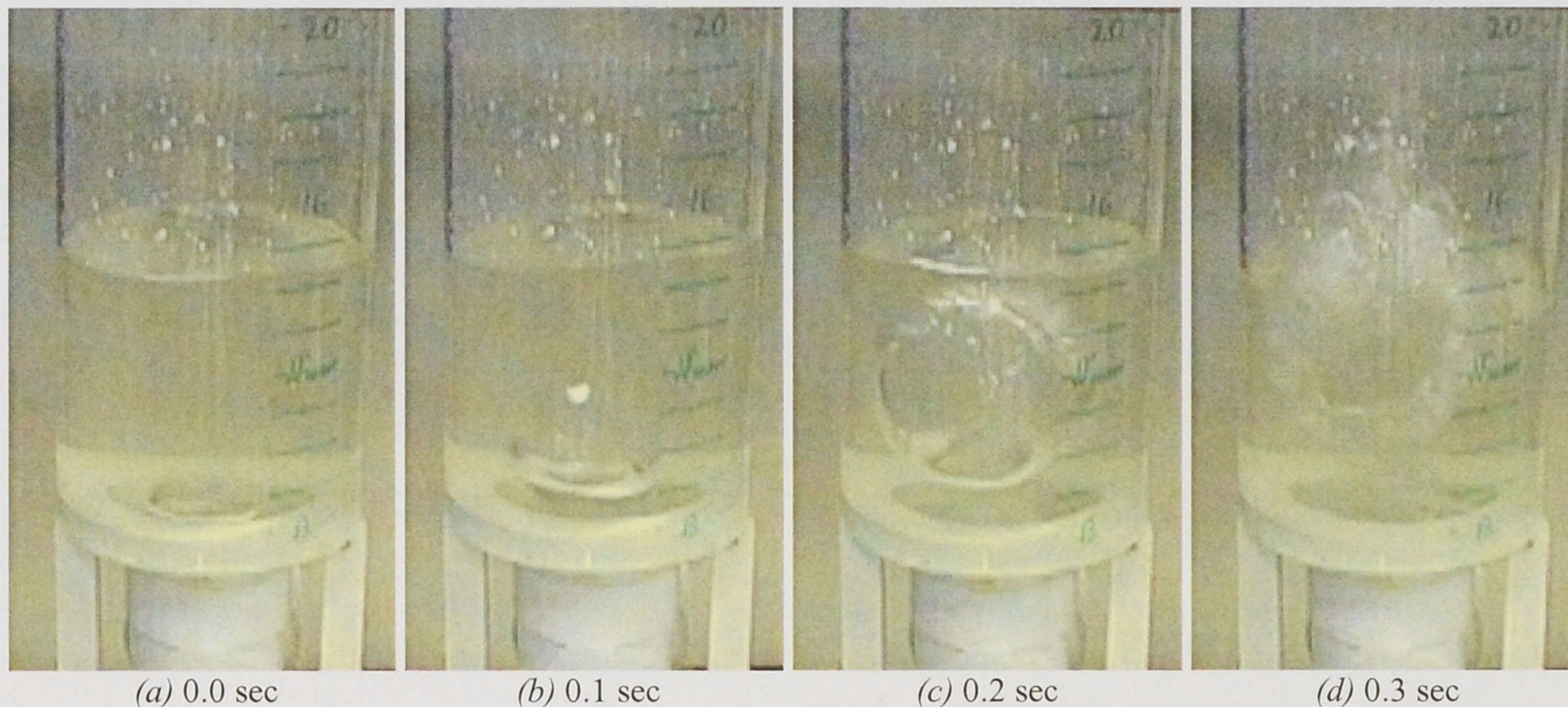


Figure 3. Images of air pocket expansion within vertical riser

3.3 Splashing

3.3.1 Constant Diameter

There are two ways to identify the strength of geyser events in these experiments. The first method, labeled “splashing”, is to observe the maximum height of any water droplets which rise due to the escaping air. The second method, labeled “inertial surge”, is to observe the maximum surface level of the water as it oscillates. In small diameter risers, the splashing effect is less noticeable because the rising air tends to form a distinct interface with the water flowing downward around it. However, for large diameter risers the air does not necessarily fill the cross section and the large air pockets project water droplets significant distances into the air as they break through the free surface. This splashing height was observed for each of the 8 trials using a 3.75 inch constant diameter riser and is listed in Table 2 along with the inertial surge levels. The height of the geyser measurements are relative to the tunnel invert and scaled from the model observations to the prototype scale based on tunnel diameter. The authors believe that the geyser strength is a function of the size of the air pocket being ventilated, but the configuration of this setup did not allow the determination of this correlation.

Geyser strength can be assessed in a number of different ways. From the observations, either the splash height or the surge height could be used as a definition. Furthermore, the measurement could be based on an absolute water rise or could be expressed relative to the initial water level in the experiment, both of which are shown in Table 2. For geysers, we believe that the splash height is more relevant

following the discussion of understood mechanisms for geyser formation discussed above. Since the splashing effect may occur as air is released through the surface and this, in turn, may occur during any phase of the surge process, in reality, the observations cannot be totally uncoupled. Indeed, the highest splashing observations corresponded with high surge levels. This was caused by a large air pocket arriving at the peak of the inertial surge rise.

It is easy to tell from Table 2 that the effect of increased air flow rate is to increase both the magnitude of splashing and surge levels. This is consistent with observations made in the previous 2008 study and we generalize these results to conclude that larger air pockets result in an increased tendency for strong geyser effects. Table 2 also shows that the relative splashing increased significantly with a higher water level within the shaft.

Table 2. Geyser measurements for constant diameter shaft control condition

(*Note: These distances are from the tunnel invert. Heights are scaled between the model and the prototype based on the diameter of the main tunnel.)

Label	Splash Height (ft., model*)	Surge Height (ft., model*)	Splash Height (ft., proto.*)	Surge Height (ft., proto.*)	Equilibrium Water Level [EWL] (ft., proto.*)	Splash Beyond EWL (ft., proto.)	Surge Beyond EWL (ft., proto.)	Splash Beyond Surge (ft., proto.)
1A	0.71	0.58	52	43	25	27	18	9
1B	0.96	0.75	71	55	25	46	30	16
2A	1.21	0.73	89	54	34.5	54	20	35
2B	1.50	0.92	110	68	34.5	76	34	43
3A	1.67	1.00	123	74	48	75	26	49
3B	1.75	1.29	129	95	48	81	47	34
4A	2.17	1.27	159	93	69	90	24	66
4B	2.25	1.52	166	112	69	97	43	54

3.2.2 Diameter Expansion

The geyser strengths for the case of a diameter expansion from 3.75 in. to 7.5 in. in the vertical shaft are shown in Table 3. Table 4 shows the reduction in geyser strength due to the diameter expansion. The maximum reduction in “splash” geyser strength, during experiment 4A, is 37 % and the average splash reduction is 17%. The maximum reduction of surge is 49% during experiment 4B and the average surge reduction is 22%. Figure 4 also shows the comparison between the geyser strengths of the constant diameter and diameter expansion results. One could interpret the relative influence of both surging and splashing among the various experiments by comparing the results in the first few columns of Table 3 to the relative changes in the sixth column (EWL). For example, the static equilibrium level change

between the 3 and 4 series of experiments is 21 feet while the change in splashing heights are similar to this change, but the surge height increases are only in the 14-17 ft range. Conversely, the static level change between the 1 and 2 series of experiments is only 8.5 ft while the increase in splash height between the two is close to 30 feet and in surge height is in the 15-20 foot range. These counteracting trends between the two series are presumed to be related to surge dynamics as discussed in more detail below. The initial water level drop in the series 1 experiments is low since the water level is close to the tunnel crown and the resulting surge is influenced by this. However, going between the series 3 and 4 experiments, the increase of initial mass in the riser provides a limit to the surge effects.

Table 3. Geyser measurements for diameter expansion

(*Note: These distances are from the tunnel invert. The expansion occurs at 0.63 ft model, 46 ft prototype. Heights are scaled between the model and the prototype based on the diameter of the main tunnel.)

Label	Splash Height (ft., model*)	Surge Height (ft., model*)	Splash Height (ft., proto.*)	Surge Height (ft., proto.*)	Equilibrium Water Level [EWL] (ft., proto.*)	Splash Beyond EWL (ft., proto.)	Surge Beyond EWL (ft., proto.)	Splash Beyond Surge (ft., proto.)
1A	0.69	0.58	51	43	25	26	18	8
1B	0.92	0.63	68	46	25	43	21	22
2A	1.08	0.77	79	57	34.5	44.5	22.5	22
2B	1.33	0.88	98	65	34.5	63.5	30.5	33
3A	1.38	0.94	102	69	48	54	21	33
3B	1.63	1.00	120	74	48	72	26	46
4A	1.71	1.13	126	83	69	57	14	43
4B	> 2.00	1.23	> 147	91	69	> 78	22	> 56

Table 4. Geyser strength reduction caused by diameter expansion

Label	% Reduction in Splash (beyond EWL)	% Reduction in Surge (beyond EWL)
1A	4	0
1B	7	30
2A	18	-15
2B	16	9
3A	28	19
3B	11	45
4A	37	42
4B	20	49
Average	17	22

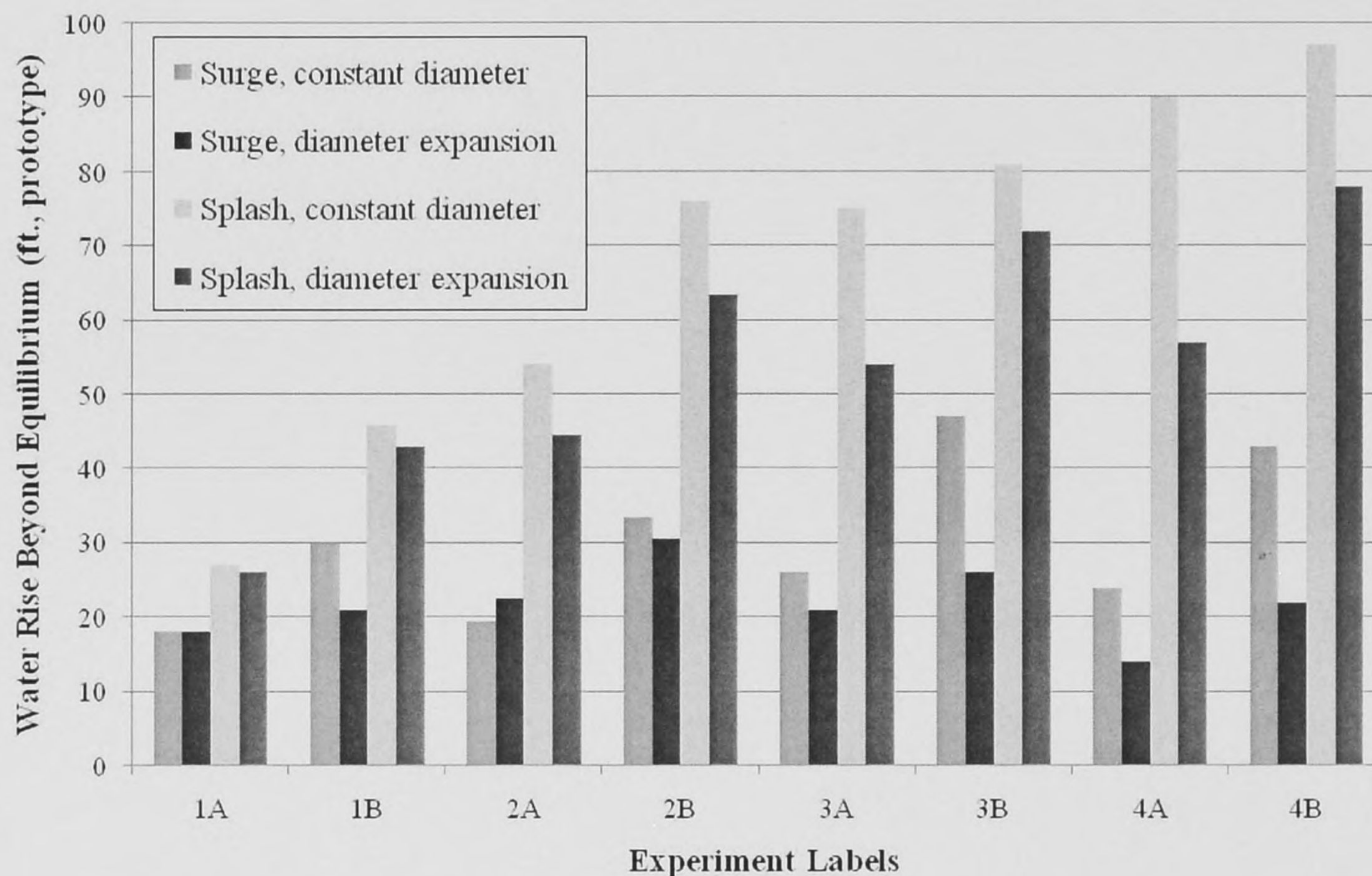


Figure 4. Geyser strengths relative to the initial water level

3.4 Scalability Concern

As discussed earlier, the flooding instability phenomenon is very difficult to produce at the laboratory scale. The velocity of the escaping air would be greater in the real system due to the scaling between the model and the prototype. The fast moving air in the real system could create enough shear at the interface with the water to entrain the water upward. The rise of this air and water mixture would therefore increase the height of the geyser compared to the laboratory observations. This phenomenon would be very important for large systems.

3.5 Inertial Surge

3.5.1 Observations

As discussed in Section 1.4, the release of a large air pocket causes the free surface in the riser to initially drop below the equilibrium level. This pressure gradient is then followed by a flow of liquid into the riser and the inertia of this liquid causes the water level to surge beyond the equilibrium point. As shown in Table 2 above, the escaping air pockets were capable of creating surge heights up to 0.41 ft (30 ft. prototype) above the equilibrium level in the shaft. Figure 4 shows that the smallest surge beyond equilibrium was experiment 4A with a value of 0.19 ft (14 ft. prototype) and the largest surge beyond

equilibrium was experiment 2B with the value mentioned of 0.41 ft (30 ft. prototype). Video observations confirmed that the largest surge levels for each experiment followed the end of a large air pocket which left the free surface level low within the riser.

3.5.2 Rigid Column Approach

A simplified numerical model which considers the inertia of the liquid in the system can be implemented to compare with the observed inertial surge. Three control volumes can be drawn as shown in Figure 5 around the liquid in the main tunnel and in each section of the riser. The length of the third control volume changes as the water level within the riser changes. The conservation of mass equations (using Eq. 1 above) can be formulated discretely based on these control volumes to obtain Eqs. 3 – 5.

$$\text{Conservation of Mass:} \quad \rho v_1 A_1 = \rho v_2 A_2 = \rho v_3 A_3 \quad (\text{Eq. 3})$$

$$\frac{d}{dt}(\rho A_3 L_3) - \rho v_3 A_3 = 0 \quad \Rightarrow \quad \frac{dL_3}{dt} = v_3 \quad (\text{Eq. 4})$$

where ρ is the constant density of water, v is the fluid velocity, and A is the cross-sectional area of the control volume perpendicular to the velocity. The cross sectional areas of the control volumes are known, allowing the velocities to be related in the following way:

$$v_1 = v_2 = 4v_3 \quad (\text{Eq. 5})$$

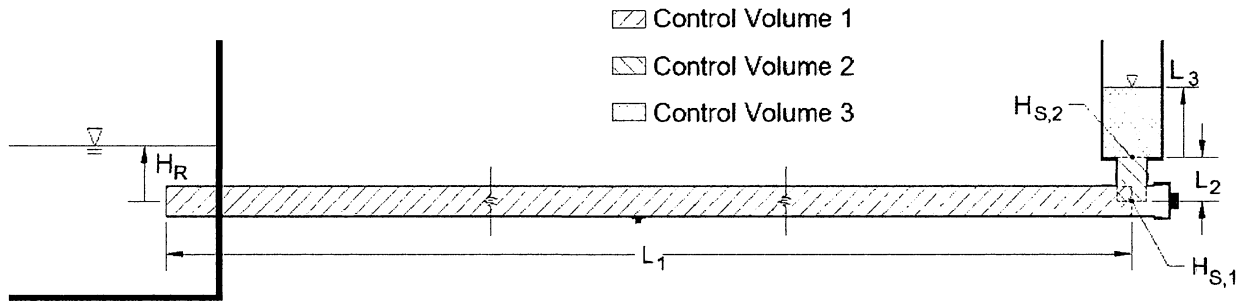


Figure 5. Sketch of the Control Volume used in the Rigid Column Method

Equations 6, 7, and 8 show the momentum relations for each of the control volumes:

$$\text{Conservation of Momentum:} \quad \rho A_1 L_1 \frac{dv_1}{dt} = \rho A_1 g (H_R - H_{S,1}) \quad (\text{Eq. 6})$$

$$\rho A_2 L_2 \frac{dv_2}{dt} = \rho A_2 g (H_{S,1} - H_{S,2} - L_2) \quad (\text{Eq. 7})$$

$$\rho A_3 L_3 \frac{dv_3}{dt} + \rho A_3 v_3 \frac{dL_3}{dt} - \rho A_3 v_3^2 = \rho A_3 g (H_{S,2} - L_3) \quad (\text{Eq. 8})$$

where H_R is the reservoir pressure head at the upstream end of the tunnel, $H_{S,1}$ is the pressure head at the base of the shaft, and $H_{S,2}$ is the pressure head at the riser expansion. The two middle terms of Equation 8 cancel based on the result of Equation 4. Matching up the pressures between the control volumes allows for the reduction of the three momentum equations to Equation 9.

$$\frac{dv_1}{dt} = \frac{g}{L_1 + L_2 + \frac{L_3}{4}} (H_R - L_3 - L_2) \quad (\text{Eq. 9})$$

Using a simple forward difference for the time derivative terms, the calculation procedure can be seen for two important variables, v_1 and L_3 below in Equations 10 and 11.

$$v_1^{n+1} = v_1^n + \Delta t \left[\frac{g}{L_1 + L_2 + \frac{L_3^n}{4}} (H_R - L_3^n - L_2) \right] \quad (\text{Eq. 10})$$

$$L_3^{n+1} = L_3^n + \Delta t \left(\frac{v_1^{n+1}}{4} \right) \quad (\text{Eq. 11})$$

It is noted that friction and local losses (due to the riser entrance and the expansion, for example) could be included in the above formulation; these would be relatively minor in terms of their effect with the resulting effect that the surge will be slightly over-predicted with this model and the period of oscillation will be slightly different as well.

3.5.2 Comparison of Numerical and Experimental Results

A specific example is used to compare the Rigid Column numerical method with the experimental measurements. The best observation of surge oscillation was during Experiment 4A because the water level stayed within the viewable range for the longest time without air interruptions. Twice during this experiment the water level dropped to a value of 0.71 ft above the tunnel invert while the reservoir level was 0.94 ft. Using initial conditions for this water level ($L_3 = 0.71 - 0.62 = 0.09$ ft) and $v_{1,2,3} = 0$, the Rigid Column approach was implemented and the results are shown in Figure 6. The observed water levels and associated time from the video are also shown in Figure 6.

Although the numerical model does fairly well to show the behavior of the surge oscillations within the riser, there are some discrepancies within the numerical framework. First, the energy losses are neglected in the Rigid Column formulation above, which would explain the slightly higher predicted

peak surge level. Energy losses would also explain the decreasing magnitude of the downward swing within the riser. Second, the fundamental period of the surge is slightly over-predicted by the Rigid Column approach. There are two possible explanations for this discrepancy. One is that our numerical model assumes that the pipe is completely full of water. In reality there is a significant amount of air at the crown of the pipe and this reduction in liquid mass would decrease the fundamental period of the oscillations. Another possible explanation is that our numerical model assumes that the velocities everywhere in the system are initially at rest. However, the continuous movement of the air pockets toward the riser somewhat reduces the validity of this assumption and could explain how the liquid in the system is able to arrive at the vertical shaft sooner than the numerical model predicts. In general, though, there is sufficient evidence to conclude that inertial surge is the physical process that is taking place within the riser to cause the oscillations.

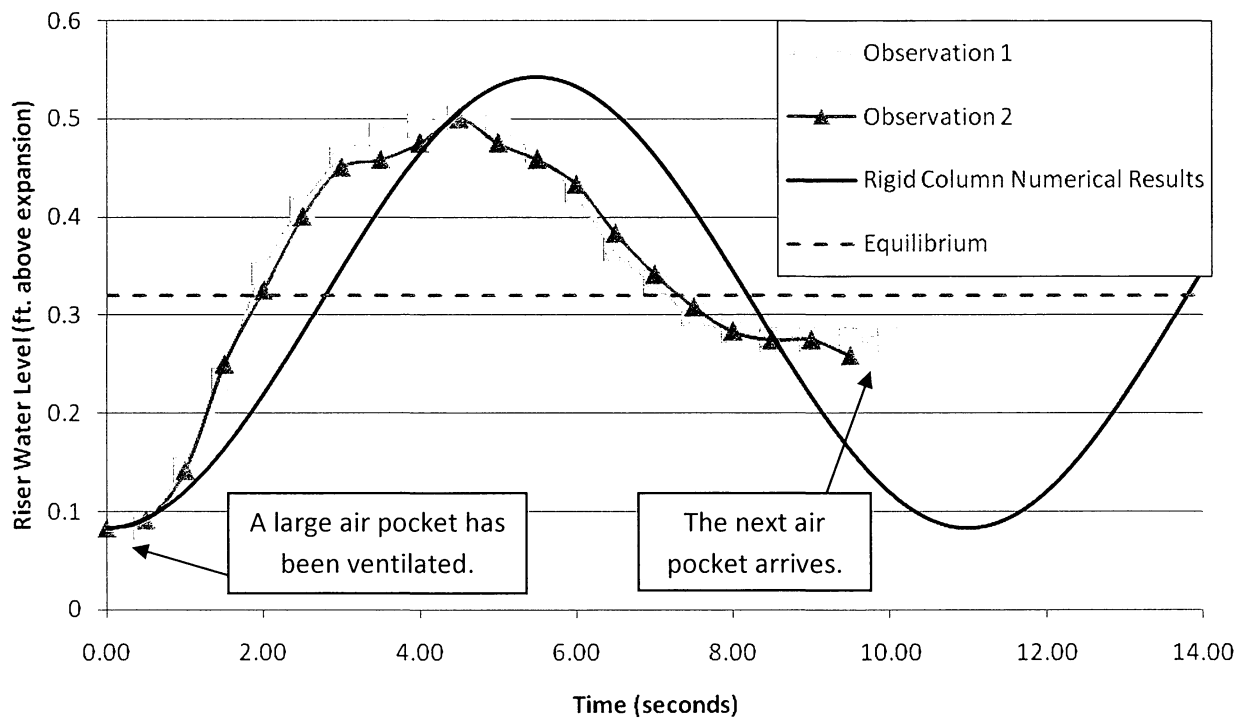


Figure 6. Comparison of Numerical and Experimental Results

The difference between the length of the physical model and the prototype tunnel would affect the inertial frequency of the oscillations. The physical model is only 77 diameters in length while the proposed prototype tunnel is hundreds of diameters in length. The increased tunnel mass in the prototype would decrease the acceleration of the liquid and lengthen the period of oscillation significantly. In other words, the large mass responds slower to local pressure changes resulting in lower peak surge values. Therefore the inertial surge within the riser due to air release is over-predicted in the physical model. As

stated above, the highest splash height typically occurs during the highest surge level, so both measures of geyser strength are expected to be over-emphasized in the physical model.

4 Conclusion

Some general conclusions can be made from the physical model investigation of the proposed 23 foot diameter CSO storage tunnel. The model was successfully constructed to represent the prototype layout based on a scaling ratio of 1:73.6.

- The expanded diameter of the vertical shaft was 7.5 in. in the model, representing 46 ft. in the prototype, which is slightly greater than the designed 45 ft diameter. This difference is negligible for evaluating the experimental results.
- The diameter expansion within the riser effectively reduced the increase of upward momentum of the air pocket by causing a radial expansion. The shaft expansion also allows for a significant amount of water to get out of the way of the rising air pockets. When compared to a constant diameter riser, the splash height is reduced by an average of 17% and the surge height is reduced by an average of 22%.
- As a large air pocket breaks through the free surface within the riser a chaotic, or churning, behavior develops as the air continues to escape.
- The geyser strength, including what is labeled “splashing” for this study, increases as the equilibrium water level increases. The buoyant air pocket accelerates longer within higher water columns, creating more upward momentum as it reaches the free surface.
- Splashing of water droplets rose significantly higher than the free surface level of the liquid.
- When scaling the air velocities up to large systems, the shear between the air and water is likely to create flooding instabilities at the interface. This important phenomenon results in an air and water mixture that would rise higher than the laboratory observations indicate.
- Once a large air pocket is released, a low local pressure may develop that initiates a flow toward the riser. The inertia of this liquid causes an overshoot of the equilibrium pressure in the system. A simple Rigid Column approach was compared to the experimental observations of a specific surge example. Small discrepancies can be explained by the assumptions of the numerical model; such as ignoring energy losses, assuming the cross section to be completely filled with water, and assuming the velocities to be initially at rest. Altogether, the general behavior of the numerical model does reveal that inertial surge is taking place within the vertical shaft.

- Inertial surge generated by the release of air pockets is expected to be less of a concern than the splashing of the geyser event in the prototype system. The increased length of the prototype tunnel system will respond slower to local pressure changes, resulting in a lower peak surge than is predicted by the model.

5 References

- Benjamin, T. B. (1968). Gravity currents and related phenomena. *J. Fluid Mech.*, 31(2), 209–248.
- Davies, R.M. and Taylor, G.I. (1950). The mechanics of large bubbles rising through extended liquids and through liquids in tubes. *Proceedings of the Royal Society of London. Series A, Mathematical and Physical Sciences*, Vol. 200, No. 1062, pp 375-390.
- Guo, Q., and Song, C. C. S. (1991). Dropshaft hydrodynamics under transient conditions. *J. of Hydr. Engrg., ASCE*, 117(8), 1042-1055.
- Hewitt, G.F. and Wallis, G.B. (1963). Flooding and associated phenomena in falling film flow in a tube. *Multiphase flow symposium winter annual meeting of ASME, Philadelphia*, (62-74).
- IIHR (2009). Iowa Institute of Hydraulic Research Draft Document, University of Iowa.
- Lewis, J.W., Wright, S.J., and Vasconcelos, J.G. (2009) “Summary of Geyser Research Experiments Conducted in the Fall of 2008 at the University of Michigan Hydraulics Lab,” Report UMCEE09-02.
- Nicklin, D.J. (1963). The air-lift pump: theory and optimization. *Transactions of the Institution of Chemical Engineers*, Vol. 41a, pp 29-39.
- Vasconcelos J.G. and Wright, S.J. (2006). Mechanisms for air pocket entrapment in stormwater storage tunnels. *Proceedings of World Water and Environmental Resources Congress, Omaha, Nebraska*, Paper 40856-14275.
- Wright, S.J. , Creech, C.T., Lewis, J.M. and Vasconcelos, J. G. (2008) “Mechanisms of Flow Regime Transition in Rapidly Filling Stormwater Storage Tunnels,” *Journal of Environmental Fluid Mechanics*, 8, 605-616.
- Wright, S.J., Lewis, J.W., Vasconcelos, J.G. (2009). Physical Processes Resulting in Geyser Formation in Rapidly Filling Stormwater Tunnels. *World EWRI Congress, May 17-21, 2009. Kansas City, MO.*

UNIVERSITY OF MICHIGAN



3 9015 09911 5217

AIIM SCANNER TEST CHART # 2

Spectra

4 PT ABCDEFGHIJKLMNOPQRSTUVWXYZabcdefghijklmnopqrstuvwxyz;"/?0123456789
 6 PT ABCDEFGHIJKLMNOPQRSTUVWXYZabcdefghijklmnopqrstuvwxyz;"/?0123456789
 8 PT ABCDEFGHIJKLMNOPQRSTUVWXYZabcdefghijklmnopqrstuvwxyz;"/?0123456789
 10 PT ABCDEFGHIJKLMNOPQRSTUVWXYZabcdefghijklmnopqrstuvwxyz;"/?0123456789

Times Roman

4 PT ABCDEFGHIJKLMNOPQRSTUVWXYZabcdefghijklmnopqrstuvwxyz;"/?0123456789
 6 PT ABCDEFGHIJKLMNOPQRSTUVWXYZabcdefghijklmnopqrstuvwxyz;"/?0123456789
 8 PT ABCDEFGHIJKLMNOPQRSTUVWXYZabcdefghijklmnopqrstuvwxyz;"/?0123456789
 10 PT ABCDEFGHIJKLMNOPQRSTUVWXYZabcdefghijklmnopqrstuvwxyz;"/?0123456789

Century Schoolbook Bold

4 PT ABCDEFGHIJKLMNOPQRSTUVWXYZabcdefghijklmnopqrstuvwxyz;"/?0123456789
 6 PT ABCDEFGHIJKLMNOPQRSTUVWXYZabcdefghijklmnopqrstuvwxyz;"/?0123456789
 8 PT ABCDEFGHIJKLMNOPQRSTUVWXYZabcdefghijklmnopqrstuvwxyz;"/?0123456789
 10 PT ABCDEFGHIJKLMNOPQRSTUVWXYZabcdefghijklmnopqrstuvwxyz;"/?0123456789

News Gothic Bold Reversed

4 PT ABCDEFGHIJKLMNOPQRSTUVWXYZabcdefghijklmnopqrstuvwxyz;"/?0123456789
 6 PT ABCDEFGHIJKLMNOPQRSTUVWXYZabcdefghijklmnopqrstuvwxyz;"/?0123456789
 8 PT ABCDEFGHIJKLMNOPQRSTUVWXYZabcdefghijklmnopqrstuvwxyz;"/?0123456789
 10 PT ABCDEFGHIJKLMNOPQRSTUVWXYZabcdefghijklmnopqrstuvwxyz;"/?0123456789

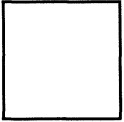
Bodoni Italic

4 PT ABCDEFGHIJKLMNOPQRSTUVWXYZabcdefghijklmnopqrstuvwxyz;"/?0123456789
 6 PT ABCDEFGHIJKLMNOPQRSTUVWXYZabcdefghijklmnopqrstuvwxyz;"/?0123456789
 8 PT ABCDEFGHIJKLMNOPQRSTUVWXYZabcdefghijklmnopqrstuvwxyz;"/?0123456789
 10 PT ABCDEFGHIJKLMNOPQRSTUVWXYZabcdefghijklmnopqrstuvwxyz;"/?0123456789

Greek and Math Symbols

4 PT ΑΒΓΔΕΕΘΗΙΚΑΜΝΟΠΦΡΣΤΥΩΧΨΖαβγδεξθηικλμνοπφρστνωχψζ≥≠",./≤±=≠' > < > < > < ≡
 6 PT ΑΒΓΔΕΕΘΗΙΚΑΜΝΟΠΦΡΣΤΥΩΧΨΖαβγδεξθηικλμνοπφρστνωχψζ≥≠",./≤±=≠' > < > < > < ≡
 8 PT ΑΒΓΔΕΕΘΗΙΚΑΜΝΟΠΦΡΣΤΥΩΧΨΖαβγδεξθηικλμνοπφρστνωχψζ≥≠",./≤±=≠' > < > < > < ≡
 10 PT ΑΒΓΔΕΕΘΗΙΚΑΜΝΟΠΦΡΣΤΥΩΧΨΖαβγδεξθηικλμνοπφρστνωχψζ≥≠",./≤±=≠' > < > < > < ≡

White



Black



Isolated Characters

e	m	1	2	3	a
4	5	6	7	o	-
8	9	0	h	l	B

MESH HALFTONE WEDGES

